Int. J. Electron. Commun. (AEÜ) 110 (2019) 152867

Contents lists available at ScienceDirect

International Journal of Electronics and Communications (AEÜ)

journal homepage: www.elsevier.com/locate/aeue

Regular paper

Frequency domain model of power amplifier for OFDM signals

A. Alkhoder *, A. Assimi, M. Alhariri

Department of Telecommunication, Higher Institute of Applied Science and Technology, Damascus, Syria

ARTICLE INFO

Article history:
Received 27 March 2019
Accepted 6 August 2019

Keywords:
Power amplifier
Nonlinearities
OFDM systems

ABSTRACT

In this paper, we present a theoretical model operating in the frequency domain of the effects of a nonlinear power amplifier on the bit error performance of orthogonal frequency-division multiplexing (OFDM) transmission systems. Based on Saleh model (Saleh, 1981), we model the in-band distortion caused by the power amplifier by an equivalent complex gain and additive white Gaussian noise. We characterize analytically the parameters of the proposed model as function of the back-off factor and the underlying parameters of the power amplifier. We demonstrate the accuracy of the proposed model by mean of numerical simulations of the bit error performance over an additive white Gaussian noise channel.

1. Introduction

In many recent wireless applications, multicarrier transmission techniques have been proposed to face frequency selectivity of the propagation channel, such as broad-band wireless local area networks [4], digital audio and video broadcasting [1,2], and interactive video services distribution [3]. More precisely, orthogonal frequency-division multiplexing (OFDM) is widely used in such systems. However, OFDM signals are very sensitive to the nonlinear distortion effects caused by the use of high power amplifiers (HPA) [5] at the transmitter. Hence, a proper design should take into account the performance degradation due to the nonlinear distortion of the transmitted signal. This distortion leads to an interference both inside and outside the signal's bandwidth. The in-band component of the interference affects the system bit error rate (BER) [6], whereas the out-of-band component affects the systems working at the adjacent frequency bands. This might be intolerable in many applications even when bit error rate (BER) degradation remains in the acceptable range [7,8].

In this paper, we only focus on the evaluation of BER degradation due to the in-band distortion caused by the HPA in OFDM systems using Quadrature amplitude modulation (QAM). The out of band radiation caused by the HPA remains outside the scope of this paper.

The motivation for this work comes from the simulation results obtained in [9,10] and [11]. It was noticed that, when HPA is used in an OFDM system, the constellation of the QAM symbols at the input of the demodulator in the receiver, is affected by two simple effects: The first one is a deterministic change, where this distortion can be viewed as a compression or an attenuation of all points in addition to a rotation of the whole constellation. This effect can be modeled by a multiplicative complex gain. The second effect has a random nature which is reflected by the presence of an additive noise (distortion noise) [9,10] and [21]. As we will see in this paper, the distortion noise can be modeled by a zero-mean complex Gaussian noise. These two effects are justified and modeled analytically in this paper. In this paper, a model for the HPA is proposed, benefiting the model proposed in [11] and [22], and justified in a theoretical framework.

While Saleh model for the HPA operates in the time domain, our model operates in the frequency domain after applying Fourier transform of the received OFDM signal. This is very useful for evaluating the BER performance of the OFDM system, where the parameters of the proposed model appears directly in the BER formula by means of introduced signal-to-noise and distortion noise ratio SNDR. This helps to directly show the effects of the underlying model of the power amplifier on system performance.

We first start our study by the system model of the OFDM transmission system considering the presence of the PA in Section 2. In Section 3, a proposed PA model is developed. In order to extract the model's parameters, the proposed model is analyzed in Section 4. In addition, the performance of the system is given analytically in term of the bit error rate in Section 4. Numerical analysis of the system is evaluated in Section 5, where, BER of the system is compared with the analytical model. The conclusion of our study is summarized in Section 6.

* Corresponding author.
E-mail addresses: assal.khoder@hiast.edu.sy (A. Alkhoder), abdelnasser.assimi@hiast.edu.sy (A. Assimi), hariri66@mail.ru (M. Alhariri).

https://doi.org/10.1016/j.aeue.2019.152867
1434-8411/

2. System model

An OFDM system is considered as a frame by frame communication system as shown in Fig. 1 [9,10] and [12]. Each frame constructs a vector of N complex symbols, $A_k,\ k = 0, 1, \cdots, N-1$, where, the symbols A_k belong to an alphabet $\mathcal{A}$ of M elements (M-QAM symbols) having the same probability and N denotes the number of OFDM subcarriers. We assume that [11,18]:

$$E[A_k] = 0, \tag{1}$$

$$E\left[A_k A_h^*\right] = \begin{cases} P, if : h = k \\ 0, otherwise \end{cases} \tag{2}$$

where $E[\cdot]$ denotes the expectation, and P is the average symbol power.

By means of the IFFT block, the frame is transformed to a vector of complex channel samples, $i_n,\ n = 0, 1, \cdots, N-1$, constructing the baseband representation of the complex envelope of the OFDM signal as [11,15,19]:

$$i_n = \frac{1}{\sqrt{N}} \sum_{k=0}^{N-1} A_k e^{\frac{j2\pi nk}{N}}. \tag{3}$$

After a suitable pulse shaping ($b(t)$ in Fig. 1) of the channel samples stream, the HPA input i_n is represented in the baseband form as [14,16]:

$$i_n = \rho_n e^{j\varphi_n}. \tag{4}$$

where ρ_n and φ_n are respectively the amplitude and phase of i_n.

When the modulated signal i_n is transmitted through the HPA (a nonlinear device), whose AM/AM and AM/PM characteristics [13,14], the output of the HPA u_n is represented in the baseband as:

$$u_n = G(\rho_n) e^{j\Psi(\rho_n)} e^{j\varphi_n}, \tag{5}$$

where $G(\rho_n)$ and $\Psi(\rho_n)$ are respectively AM/AM and AM/PM functions characterizing the HPA. Saleh model is adopted as an HPA model (it's worth noting that other than Saleh model can be adopted with the same theoretical framework followed in our study). This model, as Saleh [14] proposed, has AM/AM and AM/PM conversion functions respectively of the form:

$$\begin{aligned} G(\rho) &= \tfrac{a\rho}{1+c\rho^2}, \\ \Psi(\rho) &= \tfrac{d\rho^2}{1+e\rho^2}, \end{aligned} \tag{6}$$

where a, c, d and e are Saleh model parameters [14], ρ is the amplitude of the HPA input signal. While a is considered to be 1 as a normalized value, c, d and e are the parameters obtained using behavioral modeling of the HPA [14].

At the receiver, the received signal is filtered with the low pass filter whose impulse response is $r(t)$. The filtered signal $v(t)$ is sampled at the symbol rate to give the sampled sequence v_n, which can be written as:

$$v_n = z_n + w_n, \tag{7}$$

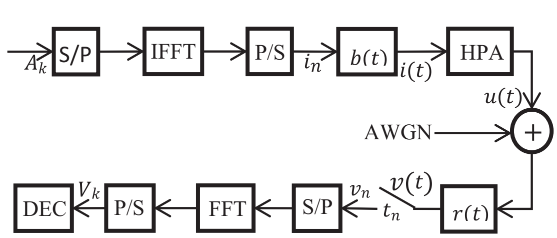

Fig. 1. OFDM system block scheme.

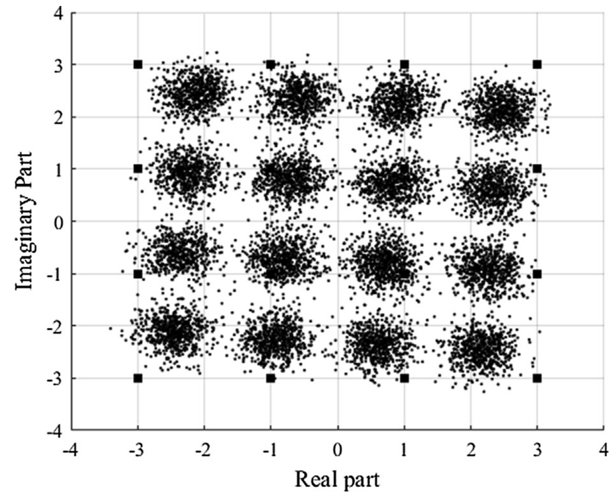

Fig. 2. Distorted received symbols, taking into account the nonlinearity of the HPA, vs. the standard 16-QAM constellation. Squares are the standard constellation and dots are the received symbols.

where z_n is the useful component and w_n is the channel noise component. v_n is then passed through FFT block to obtain the received symbols V_k which is in turn fed to the decision device DEC (QAM demodulator). Thus, the received symbols are given by [11,15,19]:

$$V_k = \frac{1}{\sqrt{N}} \sum_{n=0}^{N-1} v_n e^{-\frac{j2\pi nk}{N}}. \tag{8}$$

In order to demonstrate the effect of the HPA on the received symbols, a first simulation is performed according to the model shown in Fig. 1 without considering the channel noise w_n. The HPA used in the simulation is chosen with specific properties obtained from behavioral modeling of an amplifier fabricated by MACOM, where the corresponding Saleh model parameters were found to be: $c = 0.27$, $d = 0.3$ and $e = 3$, while $a = 1$ as a normalized linear amplification. The simulation was done for an OFDM system with 1056 subcarriers where the modulation was 16-QAM. In this case, 1056 subcarrier can be considered as a wideband signal. In addition, in existing standards, the number of subcarriers is chosen as power of two in addition to some pilot subcarriers used for the purposes of evaluating the system performance and channel quality. While we are not interested here in evaluating the overall system, the number of subcarriers is chosen arbitrarily provided that the signal can be considered as a wideband signal. Fig. 2 shows the received symbols in addition to the standard constellation corresponding to a linear amplifier. It's clear from Fig. 2 that there is a general compression or attenuation of the received symbols and a rotation angle with respect to the standard constellation, in addition to an added noise.

The error probability calculation requires the statistical characterization of the received symbol V_k. In the next sections, we provide an analytical model for the received symbols.

3. The proposed model

At the aim of creating the new proposed PA model and in order to simplify our analysis, we assume a perfect transmission chain (we ignore the effects of transmit and receive filters in addition to the channel noise) so that we start by (4) and (5), which can be rewritten at the receiver after sampling the noise-free signal as the product of terms as follows:

$$z_n = \mathscr{g}(\rho_n)\left(\rho_n e^{j\varphi_n}\right) \tag{9}$$

where $\mathscr{g}(\rho_n)$ is the nonlinear amplification of the PA given by:

$$\mathscr{g}(\rho_n) \equiv \frac{G_n(\rho_n)}{\rho_n} e^{j\Psi(\rho_n)}, \tag{10}$$

where $G_n(\rho_n)$ and $\Psi(\rho_n)$ are given by (6). After the Fourier transform of z_n, we obtain received symbols:

$$V_k = FFT(z_n) = \mathcal{G}_k * A_k, \tag{11}$$

where (*) denotes the circular convolution, and

$$A_k = FFT\left(\rho_n e^{j\varphi_n}\right), \tag{12}$$

$$\mathcal{G}_k = FFT\left(\mathscr{g}_n\right) = \frac{1}{\sqrt{N}} \sum_{n=0}^{N-1} \mathscr{g}_n e^{-\frac{j2\pi nk}{N}}. \tag{13}$$

The convolution in (11) can be written as:

$$V_k = \mathcal{G}_k * A_k = \frac{1}{N} \sum_{n=0}^{N-1} \mathscr{g}_k e^{\frac{j2\pi nk}{N}} * A_k, \tag{14}$$

where referring to (8), the received symbols at the demodulator input can be decomposed into two terms as follows:

$$V_k = A_k \mathcal{G}_0 + \frac{1}{N} \sum_{n=0, n\neq k}^{N-1} A_k \mathcal{G}_{n-k}, \tag{15}$$

where $(n-k)$ is taken modulo N. The first term in (15) corresponds to the useful symbol A_k with a multiplicative complex gain $\mathcal{G}_0$ (general compression or attenuation of the received symbols in reference to the standard constellation), and the second term corresponds to the interference coming from the other symbols and caused by the time-domain distortion (where the distortion noise in the time domain causes Inter Symbol Interference ISI in an OFDM system, which in turn causes Inter Carrier Interference in the frequency domain). The interference term $D_k$is defined by:

$$D_k \equiv \frac{1}{N} \sum_{n=0, n\neq k}^{N-1} A_k \mathcal{G}_{n-k}, \tag{16}$$

where

$$\mathcal{G}_k = \frac{1}{N} \sum_{n=0}^{N-1} \mathscr{g}_n e^{-\frac{j2\pi nk}{N}}. \tag{17}$$

4. Analytical analysis of the proposed model

We will start by describing the input of the HPA in Section III-A, and then the corresponding output in Section III-B. The proposed model's parameters are extracted in Section III-B. The model for the received symbols will be formulated in Section III-C, which leads to the floor BER performance. Finally, the BER performance is given when an AWGN channel is considered in Section III-D.

4.1. Input signal of the HPA

Depending on the nature of the signal i_n at the input of the HPA in the baseband representation (shown in Fig. 1), and by looking at (3) and (4), i_n is constructed from N independent symbols with the same statistics. Therefore, as a consequence of the central limit theorem, i_n can be considered as a complex Gaussian random process given that N is sufficiently large. In this case, the IFFT block, for large N, transforms a set of independent complex random variables to a set of complex Gaussian random variables. Therefore, the envelop of the HPA input signal ρ_n is a random process with Rayleigh distribution, and its mean and variance, when N is too large and perfect filtering ($b(t)$ in Fig. 1), are given respectively by [11,18]:

$$\beta = 0, \tag{18}$$

$$\sigma^2 = \frac{P}{N}. \tag{19}$$

This value will be used in the PA model as we will see in the later subsections.

4.2. Output signal of the HPA – Model parameters extraction

As mentioned above, there is a compression and a rotation of the whole constellation in addition to a distortion noise at the input of the demodulator. Benefiting the linearity of FFT, the output of the HPA is represented, with the use of (15), as:

$$u_n = \mathscr{g}_0 i_n + d_n, \tag{20}$$

where $d_n = \text{IFFT}(D_k)$ is the distortion noise term caused by the nonlinearity of the HPA and $\mathscr{g}_0$ is a complex gain and is independent of the input signal. This observation leads us to propose the new HPA model shown in Fig. 3.

This way, the effect of the PA on the received symbols, demonstrated shown in Fig. 2 is justified. Till now, (15) and (20) represent a new PA model in the frequency and the time domain respectively.

In order to make $\mathscr{g}_0$ and d_n mathematically tractable, d_n must be a zero-mean noise process uncorrelated with the input process i_n. Fortunately, this is justified recalling that d_n is the IFFT of D_k, going back to (15) and (16) and noting that the distortion term D_k is found when $n\neq k$. Therefore, the statistical properties of d_n could be extracted by evaluating its mean and cross-correlation with i_n, as:

$$E[d_n] = E[u_n] - \mathscr{g}_0 E[i_n] = 0, \tag{21}$$

$$E\left[d_n^* i_n\right] = E\left[u_n^* i_n\right] - \mathscr{g}_n^* E\left[i_n^* i_n\right] = 0. \tag{22}$$

This means that d_n is a zero-mean process uncorrelated with i_n. The complex constant gain in addition to the added interference terms (distortion noise) can be evaluated in the analysis demonstrated in the next subsections.

4.2.1. Complex gain calculation

Benefiting the linearity of FFT, $\mathscr{g}_0 = \mathcal{G}_0$, thus $\mathscr{g}_0$ is complex and independent of the input symbols. Therefore, the norm and angle of $\mathscr{g}_0$ are the same attenuation and rotation which affect the received symbols. These parameters could be obtained analytically.

The complex gain $\mathscr{g}_0$ can be given from (17) by:

$$\mathcal{G}_0 = \frac{1}{N} \sum_{n=0}^{N-1} \mathscr{g}_n. \tag{23}$$

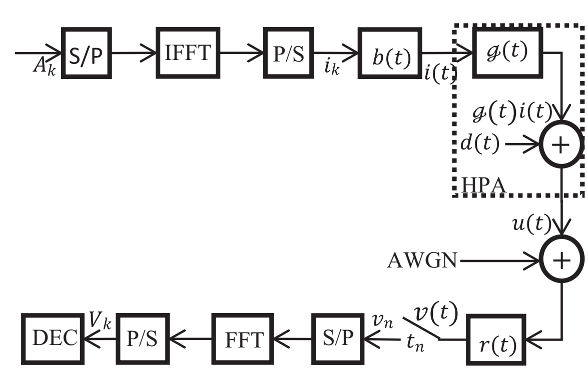

Fig. 3. OFDM system block scheme with the proposed HPA model.

For large value of N, this factor can be approximated by:

$$g_0 = \mathcal{G}_0 = E(g_n). \tag{24}$$

For the sake of brevity, ρ is adopted instead of ρ_n. Recalling (24), and reminding that ρ is Rayleigh distributed, $\mathcal{G}_0$ can be calculated in term of Saleh model parameters with the use of (6) as:

$$|\mathcal{G}_0| = E\left[\frac{G(\rho)}{\rho}\right] = E\left[\frac{a}{1+c\rho^2}\right] = \int_0^{\infty} \frac{a}{1+c\rho^2} p_\rho d\rho, \tag{25}$$

where p_ρ is the $pdf(\rho)$, then:

$$|\mathcal{G}_0| = \int_0^{\infty} \frac{a}{1+c\rho^2} \frac{\rho}{\sigma^2} e^{-\frac{\rho^2}{2\sigma^2}} d\rho, \tag{26}$$

$$|\mathcal{G}_0| = a\frac{\xi_{\mathcal{G}}}{2c\sigma^2}, \tag{27}$$

where σ^2 is given by (19), and:

$$\xi_{\mathcal{G}} = -Ei(\frac{-1}{2b\sigma^2})e^{\frac{1}{2c\sigma^2}} \tag{28}$$

where $Ei(\cdot)$ is the exponential integral. While the angle of $\mathcal{G}_0$ is evaluated with the use of (6) as:

$$\arg(\mathcal{G}_0) = \int_0^{\infty} \left(\frac{d\rho^2}{1+e\rho^2}\right) p_\rho d\rho, \tag{29}$$

$$\arg(\mathcal{G}_0) = \int_0^{\infty} \left(\frac{d\rho^2}{1+e\rho^2}\right) \frac{\rho}{\sigma^2} e^{-\frac{\rho^2}{2\sigma^2}} d\rho, \tag{30}$$

$$\arg(\mathcal{G}_0) = \frac{d}{e} + \frac{d}{2b\sigma^2}\xi_\varphi, \tag{31}$$

where

$$\xi_\varphi = Ei\left(\frac{-1}{2e\sigma^2}\right)e^{\frac{1}{2e\sigma^2}}. \tag{32}$$

4.2.2. Distortion noise variance calculation

From (15) the interference term can be rewritten as:

$$D_k = V_k - \frac{1}{N} A_k \mathcal{G}_0. \tag{33}$$

Recalling that the effect of the propagation channel is ignored, yields:

$$D_k = \mathrm{FFT}(z_n) - \mathrm{FFT}(g_n)A_k. \tag{34}$$

Benefiting the linearity of FFT, and supposing that the symbol A_k is transmitted:

$$D_k = \mathrm{FFT}(z_n - g_n A_k). \tag{35}$$

Recalling that d_n is the IFFT of D_k, and using Parseval's theorem when N is too large, we can find that:

$$E\left[|D_k|^2\right] = E\left[|d_n|^2\right]. \tag{36}$$

This means that the variances of the two interference terms at the input and output of the FFT block are the same. As the modulation symbols A_k are independent and identically distributed random variables with zero mean, the interference term D_k (16) can be then modeled by a Gaussian zero-mean random variable using the central limit theorem for large value of N. This result is verified by means of simulation. In order to check the nature of the nonlinear distortion noise components, we first plot the histogram of the real and imaginary parts of error vectors between the received symbols and the corresponding constellation points (representing the real and the imaginary parts of D_k). We can see from the simulation that these errors have the same distribution (real and imaginary parts) with the same variance. The error values are normalized to the standard constellation points in order to have a zero mean distributions, for symbols received when each symbol is transmitted for any M-QAM modulation. Fig. 4 shows the PDFs of the real or imaginary part of the mentioned error vectors. The distributions are Gaussian with a specific variance depending on the power amplifier parameters and the power input back off *IBO*, as we will see later in Section 5.

Therefore, taking (36) into account and knowing that the complex gain is independent of the input signal, the variance of the interference term can be computed from (20) by:

$$E\left[|D_k|^2\right] = E\left[|d_n|^2\right] = E\left[|u_n|^2\right] - \mathcal{G}_0^2 E\left[|i_n|^2\right]. \tag{37}$$

Supposing that $b(t)r(t) = 1$ and without considering the channel, the nonlinear distortion noise samples before FFT are $d_{rn} = d_n$. Therefore, the variance of these samples is obtained from (37) by:

$$\sigma_d^2 = E\left[|d_n|^2\right] = E\left[|u_n|^2\right] - \mathcal{G}_0^2 E\left[|i_n|^2\right]$$

$$= E\left[|S(\rho_n)|^2\right] - \mathcal{G}_0^2 E\left[|i_n|^2\right], \tag{38}$$

where $S(\rho_n) = G(\rho_n)e^{j\Psi(\rho_n)}$.

After having $|\mathcal{G}_0|$ (25), we still need to evaluate $E\left[|S(\rho)|^2\right]$ and $E\left[|i_n|^2\right]$ in order to find σ_d^2. $E\left[|S(\rho)|^2\right]$ can be calculated with the help of (6) as:

$$E\left[|S(\rho)|^2\right] = \int_0^{\infty} \left(\frac{a\rho}{1+c\rho^2}\right)^2 p_\rho d\rho, \tag{39}$$

$$E\left[|S(\rho)|^2\right] = \int_0^{\infty} \left(\frac{a\rho}{1+c\rho^2}\right)^2 \frac{\rho}{\sigma^2} e^{-\frac{\rho^2}{2\sigma^2}} d\rho, \tag{40}$$

$$E\left[|S(\rho)|^2\right] = a\frac{\xi_{\mathcal{G}} - 1}{2c^2\sigma^2} + a\frac{\xi_{\mathcal{G}}}{4c^3\sigma^4}, \tag{41}$$

Referring to (4), $E\left[|i_n|^2\right]$ can be evaluated as:

$$E\left[|i_n|^2\right] = E\left[\rho^2\right] = \int_0^{\infty} \rho p_\rho d\rho, \tag{42}$$

$$E\left[|i_n|^2\right] = \int_0^{\infty} \rho \frac{\rho}{\sigma^2} e^{-\frac{\rho^2}{2\sigma^2}} d\rho, \tag{43}$$

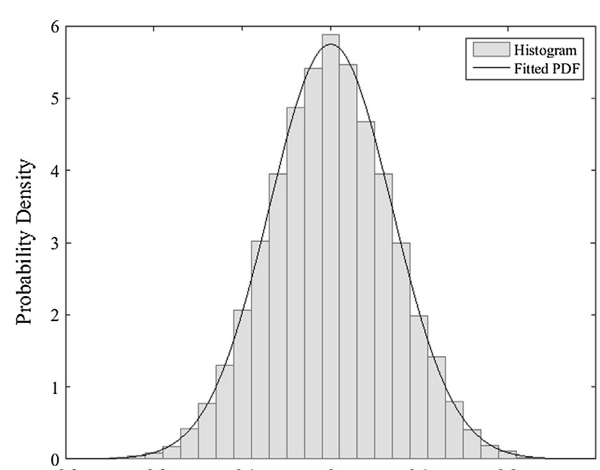

Fig. 4. PDFs of real or imaginary part of the error vector between the received symbols and the standard constellation.

$$E\left[|i_n|^2\right] = 2\sigma^2. \tag{44}$$

Therefore, substituting (27), (41) and (44) in (38), the distortion noise variance can be evaluated as:

$$\sigma_d^2 = a\frac{\xi_{\mathcal{G}} - 1}{2c^2\sigma^2} + a\frac{\xi_{\mathcal{G}}}{4c^3\sigma^4} - 2\left|a\frac{\xi_{\mathcal{G}}}{2c\sigma^2}\right|^2\sigma^2 \tag{45}$$

Keeping now the rectangular pulse shaping of $b(t)$ in mind (where the rectangular pulse shaping is considered at the aim of simplification), and knowing that i_n are zero mean Gaussian uncorrelated variables, means d_n depends only on i_n (in addition the HPA model parameters), the nonlinear distortion noise component D_k is a sum of uncorrelated random variables as in (16). Therefore, referring to central limit theorem, D_k has Gaussian real and imaginary parts whose variances can be evaluated as $\sigma_D^2 = N\sigma_d^2$.

4.3. Output signal of the FFT block

Supposing now that $b(t)r(t) = 1$, the signal at the input of FFT block ignoring the propagation channel will be:

$$z_n = g_0 i_n + d_n. \tag{46}$$

At the output of the FFT block, we obtain, after having fixed the received symbol to A_k, the input of the demodulator hence is:

$$V_k = \mathcal{G}_0 A_k + D_k, \tag{47}$$

where $\mathcal{G}_0$ is the complex gain (attenuation) affecting the constellation (given in (17)), and D_k is a noise component which has the same statistics of the noise created by the PA as it's justified in the previous section and is given in (16).

To evaluate the error probability, the pdf of nonlinearity distortion noise D_k is needed. Noting that D_k is the sum of identically distributed RVs (16), it is reasonable to assume the nonlinearity distortion noise D_k as a complex Gaussian RV, where the FFT block transforms a set of complex random variables to a set of complex Gaussian random variables. This notation is verified in the above analysis.

The BER could be evaluated starting from the decision variable at the input of the demodulator given in (47), as a function of the modulation format and the signal-to-distortion noise ratio SDR, where:

$$SDR = \frac{|\mathcal{G}_0|^2}{\sigma_D^2}. \tag{48}$$

Then BER, in our study is evaluated for M-QAM modulation where M symbols obtained by mapping $log_2(M)$ bits. Therefore BER could be evaluated by [16,17,20]:

$$P_b = \frac{2}{log_2(M)}\frac{\sqrt{M}-1}{\sqrt{M}}erfc\left(\sqrt{\frac{|\mathcal{G}_0|^2}{\sigma_D^2}}\right). \tag{49}$$

where $erfc(\cdot)$ is the error function. Up to this point, the channel is not considered. Therefore, P_b in (49) represents the floor of BER obtained in the presence of the HPA.

4.4. Considering the channel

When the channel is taken into account, an additional term must be added to the output of the FFT block containing the noise component added by the channel. Let the additional term of channel noise denoted by W_k, therefore, the input of the demodulator becomes:

$$V_k = \mathcal{G}_0 A_k + D_k + W_k, \tag{50}$$

where W_k is a Gaussian noise component whose variance is $\sigma_W^2 = N\sigma_w^2 = 2NN_0/T$. As a consequence, two noise components appears at the output of the FFT block, one of them is caused by the channel, and the other is caused by the FFT transformation after nonlinear amplification.

Therefore, the BER could be evaluated as a function of the modulation format and the signal-to-noise and distortion noise ratio SNDR. Supposing that D_k and W_k are statistically independent [19]. SNDR can be evaluated by adding the channel noise variance to the denominator of (18), as:

$$SNDR = \frac{|\mathcal{G}_0|^2}{\sigma_D^2 + \sigma_W^2}. \tag{51}$$

Then, BER is evaluated for M-QAM modulation by:

$$P_b = \frac{2}{log_2(M)}\frac{\sqrt{M}-1}{\sqrt{M}}erfc\left(\sqrt{\frac{|\mathcal{G}_0|^2}{\sigma_D^2 + \sigma_W^2}}\right). \tag{52}$$

Therefore, P_b depends on the HPA parameters and IBO in addition to the variance of channel noise.

5. Application and numerical results

Two goals are targeted in the simulations; the first goal is to verify the new proposed PA model, given in (15) or equivalently in (20), by comparing it with Saleh model, where the effects of the two models are compared in terms of the distortion noise variance and the rotation of the received symbols with respect to the standard constellation. The second goal is to verify the BER model given in (52) and comparing it with the simulation of the system when the proposed PA model is considered.

For the purpose of simplification and explaining the proceeding modeling method, the OFDM system is adopted with M-QAM modulation with rectangular waveform for $b(t)$ (as it is mentioned before the rectangular pulse shaping is adopted to simplify the analysis and the simulation at the aim of showing the effect of the power amplifier without considering other effects, while another pulse shaping can be adopted). Following the aforementioned procedure, we can evaluate the nonlinear distortion noise variance σ_D^2 in addition to the complex attenuation factor $\mathcal{G}_0$.

In the simulation, the chosen power amplifier is fabricated by MACOM. We have considered Saleh model [14] as an amplifier model to get the proposed HPA model, where a is considered to be 1 as a normalized value, c, d and e are the parameters obtained using behavioral modeling of the HPA [14], and they were found to be: $c = 0.27$, $d = 0.3$ and $e = 3$. However, in order to illustrate the effect of these parameters on the HPA behavior, the simulation was done with respect to c and $\Psi = \Psi(d, e)$ when the input back-off (IBO) changes in some region. IBO is given in dB by:

$$IBO = 10log_{10}\left(\frac{P_{max,in}}{\overline{P_{in}}}\right)[dB], \tag{53}$$

where $\overline{P_{in}} = E_b 2log_2 M/T$ is the input power of the HPA, E_b is the energy per bit. $P_{max,in}$ is maximum input power of the HPA.

The simulation was done for an OFDM system with 1056 subcarrier where the modulation was 16-QAM. We have seen in Section 4 that the real and imaginary parts of D_k have the same variance. Fig. 5 shows the changes of this variance (denoted by Xvar) with the parameter c of the amplifier for different values of IBO. It's clear from Fig. 5 that the variances decrease when c decreases, and when the IBO increases.

For the sake of simplicity, instead of studying the effect of the angle parameters d and e on the aforementioned variances, the effect of the angle Ψ itself is studied. Where, in the rest of the study

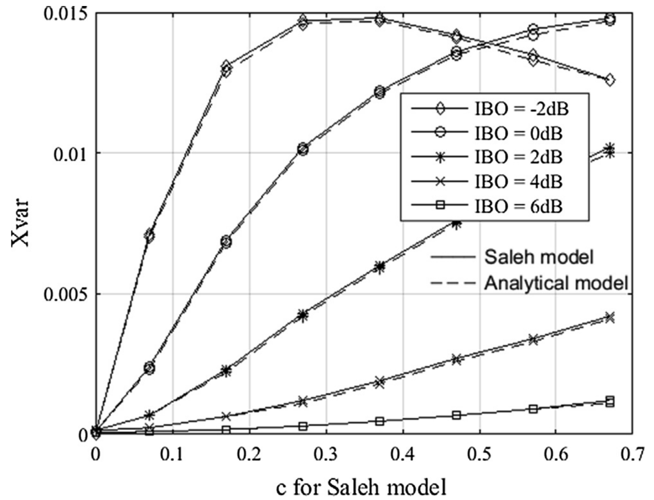

Fig. 5. The variances of the real and imaginary parts of the error vector between the received symbols and the standard constellation as function of the parameter *c* and *IBO* of the HPA.

and the simulation Ψ is taken at 1 dB compression point of the amplifier. Fig. 6 shows this effect for different values of *IBO*. We can see from Fig. 6 that there is no effect of the angle Ψ on the variances for any value of *IBO*. While *IBO* affects the variances for any value of the angle Ψ.

In addition to the variances, as we have mentioned before, the proposed model include the attenuation factor $|\mathcal{G}_0|$ and the rotation angle of the constellation. Simulation results show that $|\mathcal{G}_0|$ depends only on the parameter *c* of the HPA in addition to *IBO*. Fig. 7 shows the variations of $|\mathcal{G}_0|$ with *c* and *IBO*. From Fig. 7, we can see that $|\mathcal{G}_0|$ increases when *c* decreases and when *IBO* increases. Again the effect of the angle Ψ itself on $|\mathcal{G}_0|$ is studied. Fig. 8 shows this effect for different values of *IBO*. It's clear that there is no effect of the angle Ψ on $|\mathcal{G}_0|$ for any value of *IBO*. While *IBO* affects $|\mathcal{G}_0|$ for any value of the angle Ψ.

On the contrary, the simulation clarifies that the rotation angle of the constellation isn't affected by the parameter *c*, while it is affected by the angle Ψ. Figs. 9 and 10 show how the rotation angle of the constellation changes with *c* and Ψ. It is clear from Figs. 9

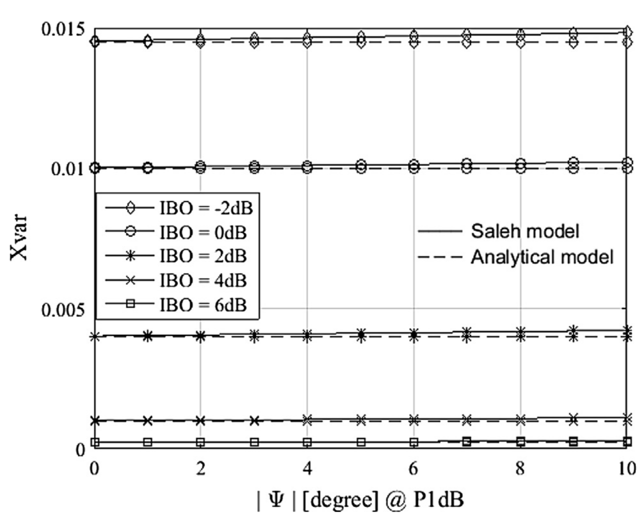

Fig. 6. The variances of the real and imaginary parts of the error vector between the received symbols and the standard constellation as function of the parameter Ψ and *IBO* of the HPA.

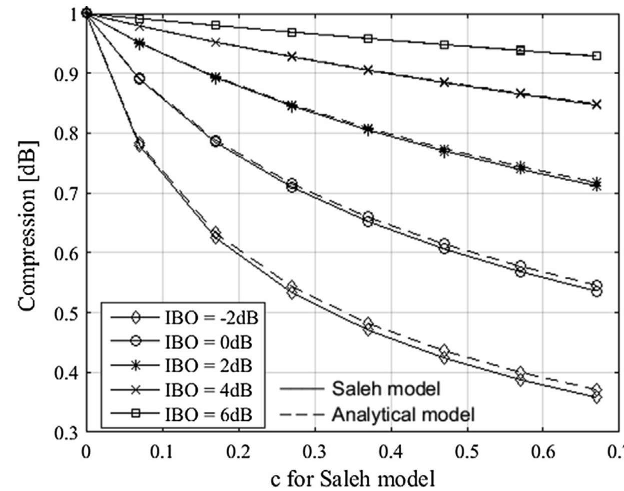

Fig. 7. Compression of the global constellation as a function of the parameters *c* and the *IBO* of the HPA.

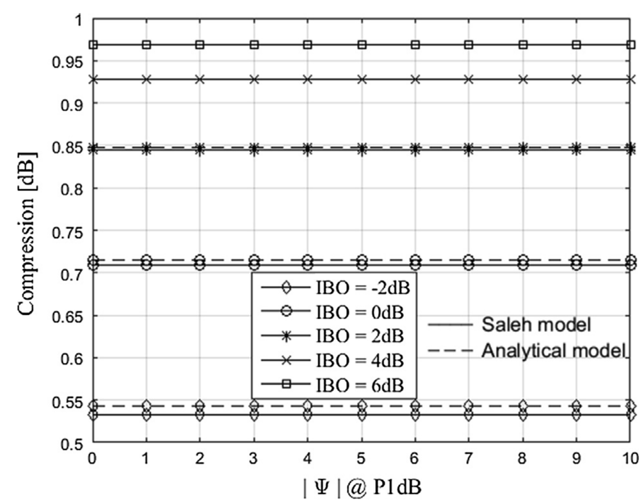

Fig. 8. Compression of the global constellation as a function of the parameter Ψ and *IBO* of the HPA.

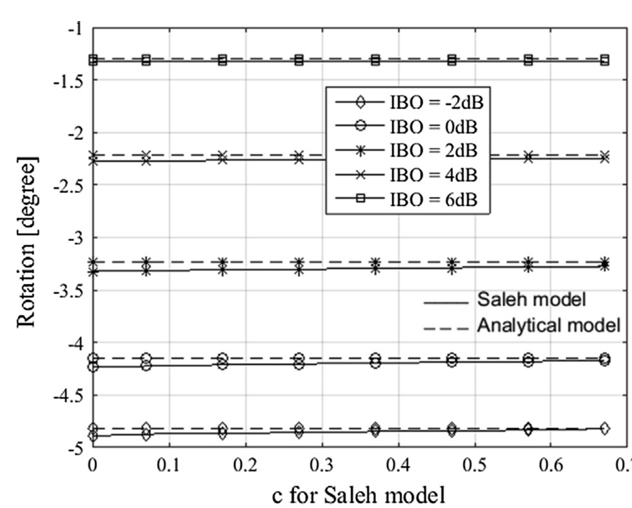

Fig. 9. Rotation angle of the global constellation as a function of the parameter *c* and *IBO* of the HPA.

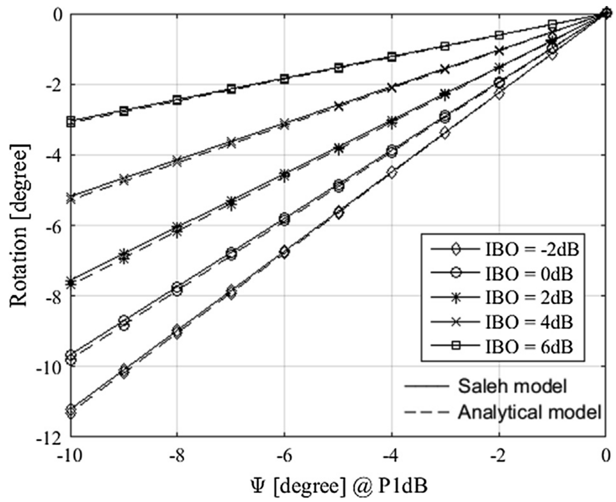

Fig. 10. Rotation angle of the global constellation as a function of the parameter Ψ and *IBO* of the HPA.

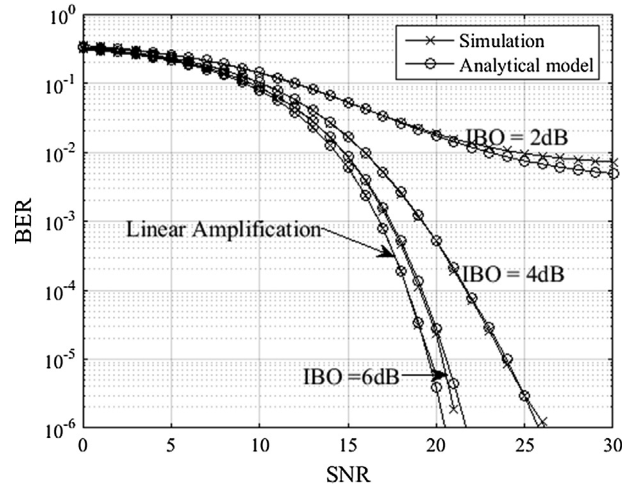

Fig. 12. BER curves vs. SNR for 16-QAM at different *IBO* values.

and 10 that the rotation angle of the constellation is affected by the angle Ψ and *IBO*, while it isn't affected by *c*.

Going back now to the proposed model of the power amplifier, which could be rewritten from (15) as:

$$u(t) = \mathcal{G}_0 i(t) + \sqrt{\sigma_D^2}(\mathcal{N}(0,1) + j\mathcal{N}(0,1)), \tag{54}$$

where $\mathcal{N}(0,1)$ is normally distributed random variable. In order to validate the proposed model, the BER curves are extracted from the simulation considering AWGN channel when the model (54) is taken into account for different values of *IBO*, and compared with the extracted analytical model (52) using identical *IBO* values. We have chosen different values of *IBO* to show if the proposed model match the analytical one. Figs. 11–14 show, at each of different *IBO* values, two BER curves vs. SNR, one of them represents the proposed PA model in (54) (or equivalently (20)) after replacing σ_D^2 from (45) (knowing that $\sigma_D^2 = N\sigma_d^2$) and $\mathcal{G}_0$ from equations (27) and (31) (the amplitude and phase of $\mathcal{G}_0$), while the other one represents the analytical model given in (52), where BER curves are obtained for different QAM modulation orders with OFDM over AWGN Channel. From Figs. 11–14, we can see the congruence between the two curves at each *IBO* value for each modulation

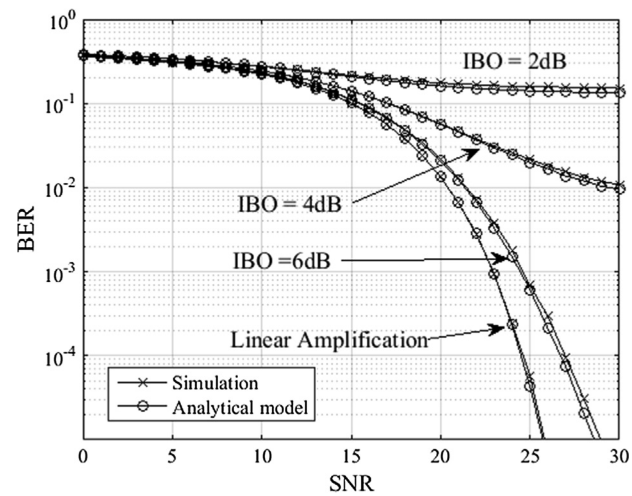

Fig. 13. BER curves vs. SNR for 64-QAM at different *IBO* values.

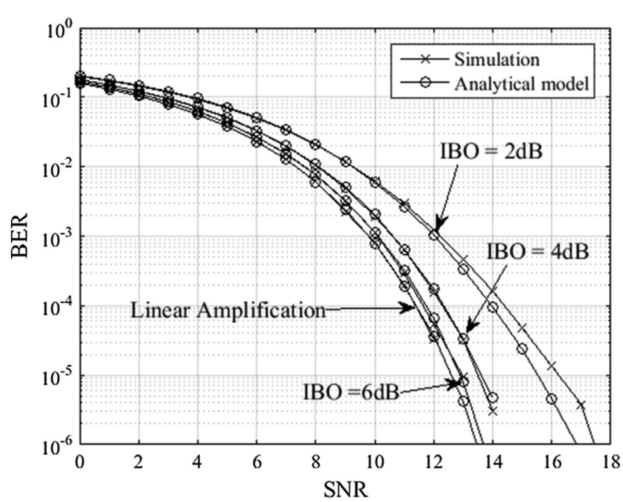

Fig. 11. BER curves vs. SNR for QPSK at different *IBO* values.

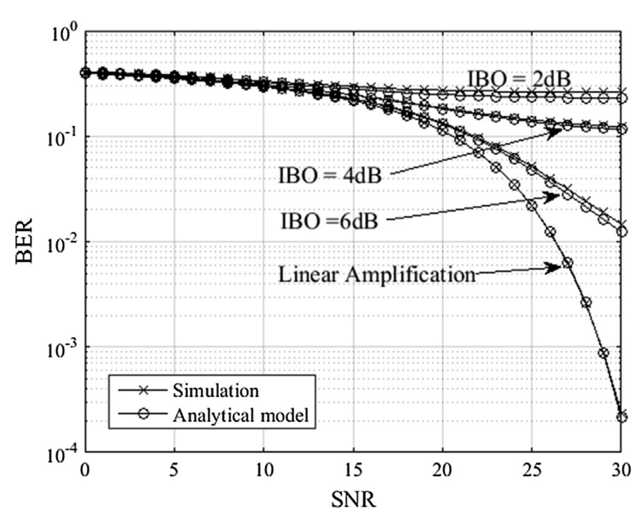

Fig. 14. BER curves vs. SNR for 256-QAM at different *IBO* values.

order, which verifies that, the proposed model is well matched with the analytical one.

6. Conclusion

An evaluation of in-band nonlinear distortion effects of band-pass memoryless nonlinear power amplifier, at the transmitter, on OFDM system, has been formulated. The power amplifier has been modeled by a complex gain in addition to added noise. Where the complex gain and the characteristics of the added distortion noise are obtained and evaluated analytically. The evaluation shows that the added noise has a Gaussian nature in its real and imaginary parts, and it has been validated numerically. In the modeling procedure, the distortion noise characteristics functionalities of the Saleh model parameters are extracted in order to formulate the model. As a consequence of this modeling method, an analytical evaluation of error probability has been extracted. The accuracy of the proposed model has been validated for an OFDM system with a specific power amplifier. Simulation results confirm the agreement between the proposed model for the power amplifier and the analytical form, where bit error rate is chosen as a performance criterion. As a future work, this method of modeling could be applied to power amplifier models other than Saleh one in order to evaluate the accuracy of distortion noise characteristics and to find out if other models can lead to models simpler than the proposed one, which may facilitate the study of the nonlinearity compensation of the nonlinear amplifier. In addition, this developed methodology could be extended to evaluate the effect of nonlinearity out-of-band using spectral analysis.

Declaration of Competing Interest

No conflict of interest.

References

[1] Le Floch B, Halbert-Lassalle R, Castelain D. Digital sound broadcasting to mobile receivers. IEEE Trans Consumer Electron Aug. 1989;35:493–503.

[2] Terrestrial Digital Video Broadcasting. ETSI specification, EN 300 744.

[3] Tralli V, Vaccari A, Verdone R, Andrisano O. Adaptive C-OFDM system at 30 GHz for the last mile wireless broadband access to interactive services. In: Proc IEEE ICC'98, Atlanta, GA; June 1998. p. 1314–9.

[4] Dardari D, Tralli V. High-speed indoor wireless communications at 60 GHz with coded OFDM. IEEE Trans Commun Nov. 1999;47:1709–21.

[5] Chini A, Wu Y, El-Tanany M, Mahmoud S. Hardware nonlinearities in digital TV broadcasting using OFDM modulation. IEEE Trans Broadcast Mar. 1998;44:12–20.

[6] O'Neil R, Lopes LB. Performance of amplitude limited multitone signals. In: Proc IEEE VTC'94, Stockholm, Sweden; June 1994. p. 1675–9.

[7] Li X, Cimini LJ. Effects of clipping and filtering on the performance of OFDM. In: {rpc/IEEE VTC'97, Phoenix, AZ; May 1997. p. 1634–8.

[8] May T, Rohling H. Reducing the peak-to-average power ratio in OFDM radio transmission systems. In: Proc. IEEE VTC'98. Canada: Ottawa, ON; May 1998. p. 2474–8.

[9] Brajal A, Chouly A. Compensation of nonlinear distortions for orthogonal multicarrier schemes using predistortion. In: Proc IEEE GLOBECOM'94, San Francisco, CA; Nov. 1994. p. 1909–14.

[10] Santella G, Mazzenga F. A hybrid analytical-simulation procedure for performance evaluation in M-QAM-OFDM schemes in presence of nonlinear distortions. IEEE Trans Veh Technol Feb. 1998;47:142–51.

[11] Dardari D, Tralli V, Vaccari A. A theoretical characterization of nonlinear distortion effects in OFDM systems. IEEE Trans Commun Oct. 2000;48(10).

[12] Weinsten SB, Ebert PM. Data transmission in frequency division multiplexing using the discrete Fourier transform. IEEE Trans Commun Oct. 1971;COM-19.

[13] Benedetto S, Biglieri E, Castellani V. Digital transmission theory. Englewood Cliffs, NJ: Prentice-Hall; 1987.

[14] Saleh AAM. Frequency independent and frequency dependent nonlinear model of TWT amplifiers. IEEE Trans Commun Nov. 1981;COM-29:1715–20.

[15] Bohara VA, Ting SH. Theoretical analysis of OFDM signals in nonlinear polynomial models. 6th International conference on information, communications & signal processing; Dec. 2007.

[16] Zareian H, Vakili VT. Analysis of nonlinear distortion using orthogonal polynomials HPA model. Int J Comput Sci Network Security Jan 2008;8(1).

[17] Banelli P. Theoretical analysis and performance of OFDM signals in nonlinear fading channels. IEEE Trans Wireless Commun March 2003;2(2):284–93.

[18] Rudziński A. Normalized Gaussian approach to statistical modeling of OFDM signals. J Telecommun Inform Technol March 2014;1:54–61.

[19] Iofedov I, Wulich D. On OFDM-MRT with nonlinear power amplifier. 2014 IEEE 25th annual international symposium on personal, indoor, and mobile radio communication (PIMRC); 2-5 Sept. 2014. p. 512–6.

[20] Ermolova NY. M-QAM OFDM system performance in the presence of nonlinear and frequency offset effects. 2005 IEEE 16th international symposium on personal, indoor and mobile radio communications, vol. 2; 11-14 Sept. 2005. p. 1120–4.

[21] Araújo T, Dinis R. On the accuracy of the gaussian approximation for the evaluation of nonlinear effects in OFDM signals. IEEE Trans Commun Feb 2012;60(2):346–51.

[22] Lajnef H, Dakhli MC, Hizem M, Bouallegue R. The effect of the nonlinear distortion on OFDM based cognitive radio systems over rayleigh fading channel. 2016 30th International conference on advanced information networking and applications workshops; 23-25 March 2016.

A. Alkhoder, was born in Damascus, Syria in 1978. He received the B.Eng. Degree in electronic engineering from Albaath university, Homs, Syria in 2002, diploma of Higher studies in communications Engineering from Damascus University in 2003, and M.S. degree in high frequency materials and components for communication systems from Université de Bretagne Occidentale (UBO), Brest, France, in 2010. He is currently working towards the Ph.D. degree at the Higher Institute for Applied Sciences and Technology, Damascus, Syria. His research interests are on Enhancing wireless communication systems.

A. Assimi, was born in Derra, Syria in 1973. He received the Eng. degree from the ENST, Paris, France in 1996 and the Ph.D. degree from the University of Cergy-Pontoise, Cergy-Pontoise, France in 2009. He is currently an Assistant Professor and Head of Digital Electronics Lab at the Higher Institute for Applied Sciences and Technology, Damascus, Syria. His research interests include Man-Machine communication, mobile communication, and Turbo-processing and its application to communication systems.

M. Alhariri, was born in Damascus Syrian Arab Republic in 1966. Received the electrical engineering degree in 1991 from the Damascus University. He received his Master degree in Antennas and Microwave Device at the Bauman Moscow State Technical University in 1997. He received his Ph.D. degree in Antennas, microwave devices and their technologies at the Moscow Aviation Institute in 2007. His research interests are in Electrodynamics modeling of printed slit antennas. He work in the Higher Institute of Applied Science and Technology in Damascus (HIAST-Syria).